

Review

# Progress of Photonic-Crystal Surface-Emitting Lasers: A Paradigm Shift in LiDAR Application

Yu-Heng Hong <sup>1</sup>, Wen-Chien Miao <sup>1,2</sup>, Wen-Cheng Hsu <sup>1</sup>, Kuo-Bin Hong <sup>1</sup>, Chun-Liang Lin <sup>2</sup>, Ching Lin <sup>3,\*</sup>, Shih-Chen Chen <sup>1,\*</sup> and Hao-Chung Kuo <sup>1,4</sup>

<sup>1</sup> Semiconductor Research Center, Hon Hai Research Institute, Taipei 11492, Taiwan; enoch.yh.hong@foxconn.com (Y.-H.H.); leona.wc.miao@foxconn.com (W.-C.M.); wen-cheng.hsu@foxconn.com (W.-C.H.); robin.kb.hong@foxconn.com (K.-B.H.); hckuo@faculty.nctu.edu.tw (H.-C.K.)

<sup>2</sup> Department of Electrophysics, College of Science, National Yang Ming Chiao Tung University, Hsinchu 30010, Taiwan; clin@nycu.edu.tw

<sup>3</sup> Science & Technology Policy Research and Information Center, National Applied Research Laboratories, Taipei 10636, Taiwan

<sup>4</sup> Department of Photonics, Institute of Electro-Optical Engineering, College of Electrical and Computer Engineering, National Yang Ming Chiao Tung University, Hsinchu 30010, Taiwan

\* Correspondence: clin@narlabs.org.tw (C.L.); gary.sc.chen@foxconn.com (S.-C.C.)

**Abstract:** Nowadays, the flurry of autonomous vehicles is in full swing regarding light detection and ranging (LiDAR) and depth perception. For such visual perception, light plays an important role. We human beings recognize and distinguish surrounding details when the eye focuses light on the retina. For the LiDAR system, pulsed lasers are employed to measure the relevant range. Thus, appropriate light sources with high performance are in urgent demand. Auspiciously, a revolutionary semiconductor laser technology, namely the photonic-crystal surface-emitting laser (PCSEL), emerges over the past two decades. PCSEL exhibits not only a symmetric beam profile with narrow beam divergence but also a high-power operation with controllability. Therefore, it may be the holy grail for an ultracompact time-of-flight (ToF) LiDAR system. Hereupon, comprehensive analyses of PCSEL-relevant scientific publications and patent documents are conducted. We thereby review the development progress of PCSEL technology. Moreover, a systematic simulation is performed, providing real-time visualization of relevant point clouds with different beam divergence. PCSEL technology with unprecedented merits indeed turns a new leaf and a paradigm shift in LiDAR application is ongoing. It is believed that a lens-free and adjustment-free ultracompact apparatus in simplicity can be expected.

**Keywords:** photonic-crystal surface-emitting laser; PCSEL; light detection and ranging; LiDAR



**Citation:** Hong, Y.-H.; Miao, W.-C.; Hsu, W.-C.; Hong, K.-B.; Lin, C.-L.; Lin, C.; Chen, S.-C.; Kuo, H.-C. Progress of Photonic-Crystal Surface-Emitting Lasers: A Paradigm Shift in LiDAR Application. *Crystals* **2022**, *12*, 800. <https://doi.org/10.3390/cryst12060800>

Academic Editor: Dmitri Donetski

Received: 4 May 2022

Accepted: 31 May 2022

Published: 6 June 2022

**Publisher's Note:** MDPI stays neutral with regard to jurisdictional claims in published maps and institutional affiliations.



**Copyright:** © 2022 by the authors. Licensee MDPI, Basel, Switzerland. This article is an open access article distributed under the terms and conditions of the Creative Commons Attribution (CC BY) license (<https://creativecommons.org/licenses/by/4.0/>).

## 1. Introduction

Light is a vital element throughout the day, for we human beings, allowing us to recognize surrounding things and distinguish the further details. Additionally, for machine vision and intelligence, light detection and ranging (LiDAR) and depth perception are nowadays experiencing a flurry of interest in autonomous vehicles, videlicet the self-driving cars [1,2]. The expeditious needs for miniature devices with multi functionalities are in urgent demand. For laser light sources toward the ultracompact time-of-flight (ToF) LiDAR system, schematic illustration of various laser modules and relevant development progress, are shown in Figure 1.

The edge-emitting laser (EEL), as a Fabry–Pérot semiconductor laser, is the most common choice. However, laser light emission from EELs usually suffers from several undesirable features, such as a broad lasing spectrum, an inherent edge-emitting direction, an asymmetric beam profile, and a large beam divergence. Thus, requiring a complicated lens

system attempts to tackle the aforesaid drawbacks. Such a complicated lens system not only needs fine adjustment but also leads to a bulky form factor, running counter to the miniaturization trend of consumer electronics and devices. In 1988, the first room-temperature laser light emission from a vertical-cavity surface-emitting laser (VCSEL) was demonstrated, and some drawbacks of EELs can be thereby solved with the symmetric beam profile and narrow spectrum, increasing the various applications with this kind of laser light source [3–13]. Owing to the distinct structural design, laser light emission from a VCSEL is perpendicular to the mounting surface with a circular beam profile, thus reducing the demand for a complicated lens system for beam shaping. However, the requisite for out-put beam collimation is yet to remain, due to the unsatisfactory beam divergence and the multimodal lasing oscillation in high-power operation.

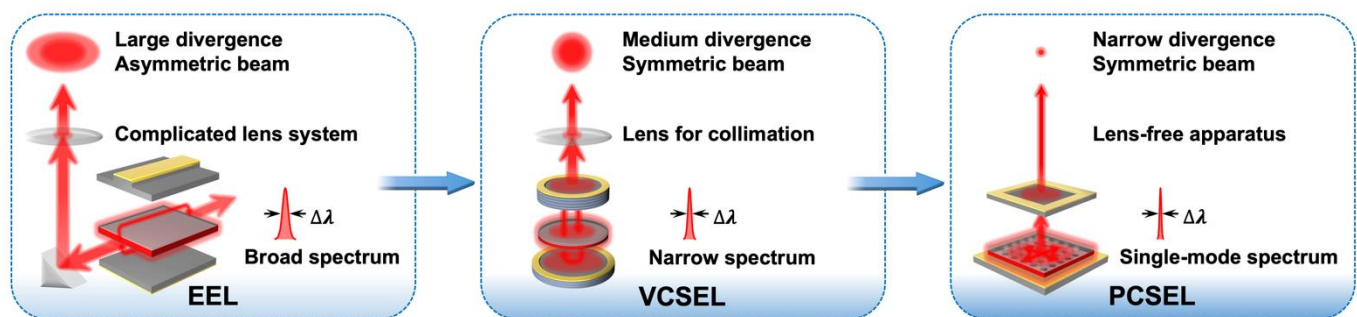


**Figure 1.** Schematic illustration for the development progress of laser light sources.

Considering the perspective of miniaturization, ultracompact optical devices with miscellaneous functionalities and new concepts are in the urgent stage of rapid development to ameliorate the bulky form factor of common optical devices. Typically, traditional optical devices, such as lenses, can focus or disperse a light beam by means of refraction. Nevertheless, artificial structures fabricated at the micro- or nanoscale, such as photonic crystals, can use the periodical changes of material refractive index to affect the propagation of a light beam, imitating natural crystals that give rise to the X-ray diffraction with their atomic lattices. Thus, with this kind of artificial structure, photonic crystals can pave prospective ways for specific light modulation with ultracompact form factors.

Auspiciously, thanks to the monolithic integration of photonic crystals embedded in the epitaxial structures, a revolutionary semiconductor laser technology nowadays turns over a new leaf. With the monolithic integration, a photonic crystal can be adopted as a lateral laser cavity, generating a photonic-crystal surface-emitting laser (PCSEL) [14,15]. Through the band-edge resonance of embedded photonic crystal, laser light emission from a PCSEL exhibits a high-power single-mode operation with controllability. Moreover, such a laser light emission presents a symmetric beam profile with narrow beam divergence and spectral width [16,17]. Altogether, PCSEL is quite suitable for the LiDAR application, enabling a lens-free and adjustment-free apparatus [18–20].

To gain a deeper understanding of the overall development progress for PCSEL technology fronts, we first conduct comprehensive analyses of PCSEL-relevant scientific publications after the proposed concept of photonic crystals and patent documents retrieved from Clarivate Analytics' Web of Science (WoS) bibliometric database and Derwent Innovation's patent database, respectively [21–24]. Subsequently, we review the recent development progress of PCSEL technology. Finally, a systematic simulation of different beam divergence is conducted, providing real-time visualization of relevant point cloud results. Based on the development progress in PCSEL, a paradigm shift in LiDAR application is ongoing with this revolutionary semiconductor laser technology. Thus, it is believed toward a lens-free and adjustment-free ultracompact apparatus in simplicity can be expected.

## 2. Analysis of PCSEL Technology Fronts

Statistical data of PCSEL-relevant scientific publications and patents were retrieved and analyzed in this section. Hence, these analyses can offer a broad perspective on the overall development progress of PCSEL technology fronts as well as a forecast for the ongoing trend of practical uses.

### 2.1. Methodology

The scientific publications, 670 documents published before 8 April 2022, types of which included articles, review articles, and proceeding papers, were retrieved from Clarivate Analytics' Web of Science (WoS) bibliometric database [23]. Exact phrases of "photonic-crystal" and "surface-emitting" and the wildcard of laser, namely "laser\*", were used as the search term and queried in "topic," i.e., the union of publications' title, abstract, and keywords. Regarding the relevant patents, the same search term, i.e., exact phrases of "photonic-crystal" and "surface-emitting" and the wildcard of laser, was queried in patents' all text fields, comprising title, abstract, claims, and description, to retrieve the patents or patent applications across all patent offices around the world, (e.g., United States Patent and Trademark Office, China National Intellectual Property Administration, Japan Patent Office, etc.), through Derwent Innovation's patent database [24]. Thereby, 4609 patents or patent applications published before 8 April 2022 were retrieved.

### 2.2. Overview of Relevant Publications from Web of Science (WoS)

The idea and device of PCSEL were first proposed in 1999 in the paper titled "Coherent two-dimensional lasing action in surface-emitting laser with triangular-lattice photonic crystal structure," authored by Masahiro Imada, Susumu Noda, Alongkarn Chutinan, and Takashi Tokuda, which was unsurprisingly the most cited research article of PCSEL (cited 570 times). The others within the top five cited PCSEL research articles were "Ultralow-threshold electrically pumped quantum-dot photonic-crystal nanocavity laser" published in 2011 (cited 320 times), "Watt-class high-power, high-beam-quality photonic-crystal lasers" in 2014 (cited 278 times), "GaN photonic-crystal surface-emitting laser at blue-violet wavelengths" in 2008 (cited 249 times), and "Quantum cascade surface-emitting photonic crystal laser" in 2003 (cited 248 times).

Initially, PCSEL technology welcomed a progressive publication period from 1999 to 2007, during which the annual publication counts grew from 7 in 1999 to 50 in 2007, as shown in Figure 2a. Later, a publication plateau was kept for 6 years until 2013. PCSEL has kept its research momentum since then. The top five authors published the most in the area of PCSEL were Susumu Noda from Kyoto University, Japan, Kent D. Choquette from the University of Illinois, USA, Tien-Chang Lu from National Chiao Tung University, Taiwan, Maciej Dems from the Technical University of Lodz, Poland, and Weidong Zhou from the University of Texas at Arlington, USA, as shown in Figure 2b. Among them, S. Noda was the most dedicated contributor who, every year, authored an average of four relevant articles with an accumulated publication count of 89 since the very first article in 1999.

In addition, as shown in Figure 3, most of the PCSEL articles were published in the USA (175 publications), Japan (143), China (75), Taiwan (71), England (52), and France (52), etc. The publication rank reveals that Taiwan, whose population base is far less than the other highly ranked, has great developing potential in the PCSEL research area and is very competitive.

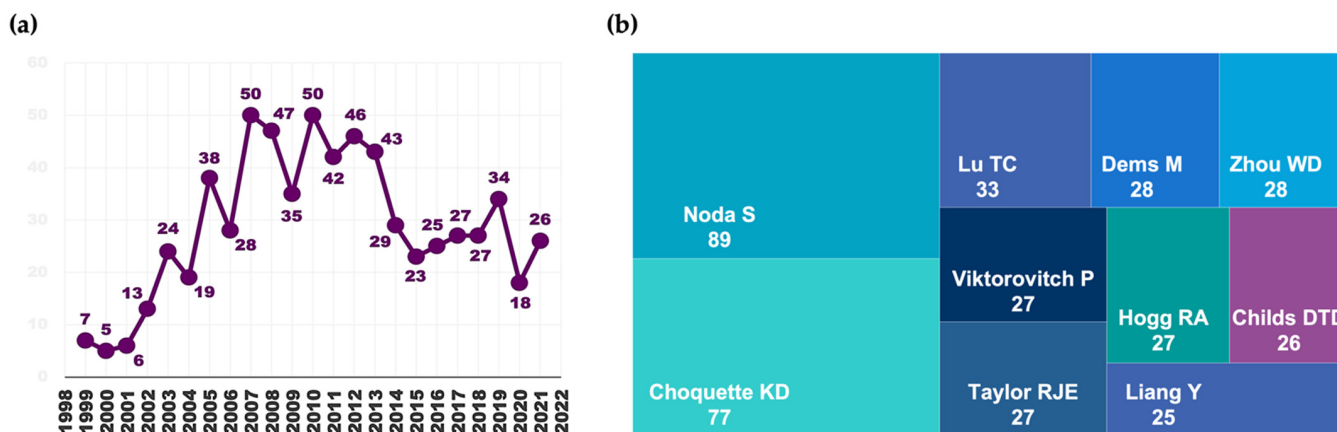


Figure 2. Overview of relevant publications retrieved from Clarivate Analytics’ Web of Science (WoS) bibliometric database. (a) The corresponding annual publication counts. (b) The top 10 authors contributing the most to the area of PCSEL.

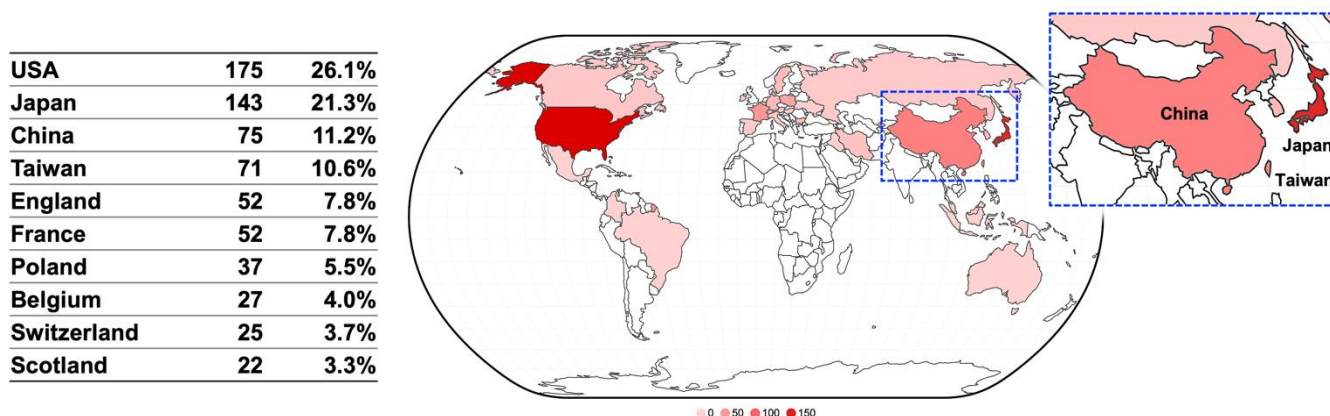
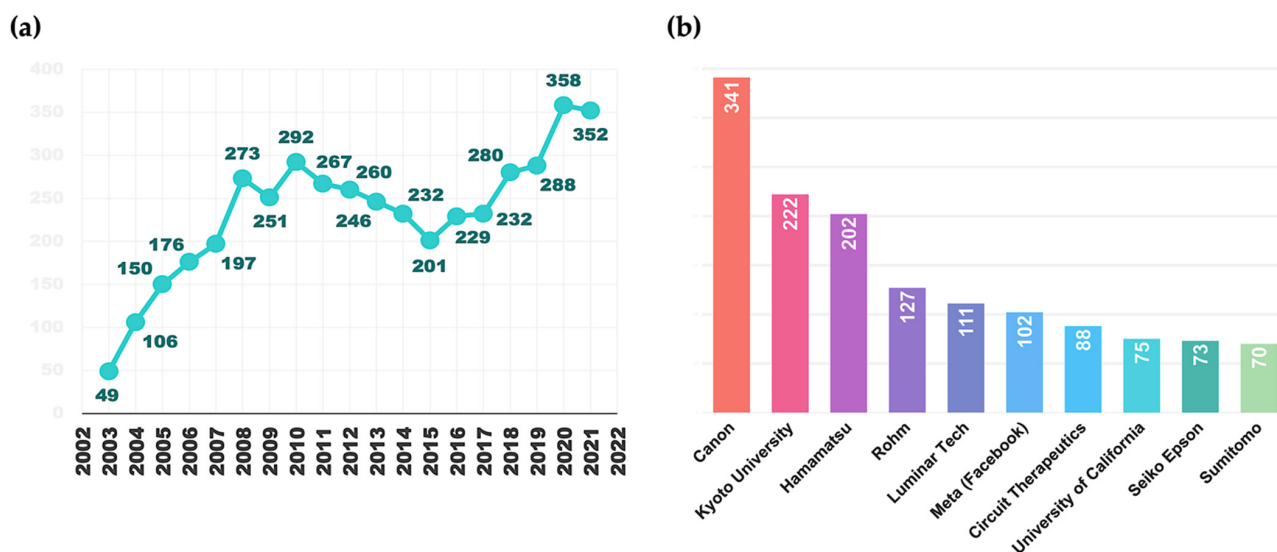


Figure 3. The top 10 countries contributing the most to the area of PCSEL and the corresponding world choropleth map for the relevant publications retrieved from Clarivate Analytics’ Web of Science (WoS) bibliometric database. **Inset:** A zoom-in view of Taiwan (blue dashed line square), whose population base is far less than the other highly ranked, has the competitive potential in the PCSEL research area.

### 2.3. Overview of Relevant Patents around the World

A total of 1540 of the retrieved 4609 patent documents were granted patents, and the other 3069 were patent applications. The grant rate of PCSEL-relevant patents (1540/3069) is lower than the average grant rate of ~70% for all patents around the world. The 4609 documents belonged to 1531 patent families, which means there were only 1531 inventions used to apply for 3069 patent applications across patent offices of different countries.

As shown in Figure 4a, the relevant patent counts linearly grew from 49 in the year 2003 to 273 in 2008. This trend was like that of scientific publications. The PCSEL patenting activity later faced a stagnant period from 2008 to 2015; however, unlike the latest slightly downward trend of PCSEL research publications (see Figure 2a), the PCSEL-relevant annual patent counts kept growing again in 2015, which implies that lots of practical uses of PCSEL had been rapidly developed.



**Figure 4.** Overview of relevant patents retrieved from Derwent Innovation’s patent database. (a) The corresponding annual patent counts. (b) The top 10 PCSEL-relevant patent assignees.

Figure 4b shows the top 10 PCSEL-relevant patent assignees ranked by the sums of their patents and patent applications. The concept of PCSEL was first proposed by the Japanese, and the top four assignees were the “origin” of PCSEL, Kyoto University, and Japanese companies including Canon, Hamamatsu, and Rohm. Accordingly, the top six PCSEL-relevant patent application countries/regions were the United States, Japan, China, Europe, Korea, and Taiwan, which implies that the most PCSEL-relevant inventions were likely to be implemented in those countries.

### 3. Progress in PCSEL Technology

The concept of photonic crystals was independently proposed by E. Yablonovitch and S. John in 1987 [21,22]. Afterward, this kind of artificial structure with photonic bandgaps attracted much attention for their special dispersion. As an analogy to the quantum mechanics of electrons in a natural crystal, a photonic crystal uses the periodical changes in the refractive index of composed dielectric materials as an artificial crystal, and thus exhibits a photonic band structure. As a result, for such a photonic band structure, a photonic bandgap exists in between these bands, like the semiconductor bandgap in solid-state physics.

Accordingly, within these bands, the transmission of light beams is strictly inhibited, hence forming the forbidden bands. In early 1946, the enhancement effect for the spontaneous emission rate of a quantum system can be achieved by its environment, such as by exploiting a microcavity [25]. Thereafter, relevant discussion on the coupling between electromagnetic fields and materials is well known as the Purcell effect, named after E. M. Purcell. Taking advantage of these bands for light inhibition, an engineered cavity with the reduction of corresponding mode volume can be accomplished; therefore, a bandgap type of photonic crystal for lasing is possible. Due to the volume reduction of such engineered micro- or nanocavity, the eventual number of modes supported by the bandgap type of photonic crystals can be decreased, resulting in a dramatically increased spontaneous emission coupling coefficient [26]. Thus, in 1996, relevant lasing actions in such bandgap types of photonic crystals can be observed with an ultra-low lasing threshold, even theoretically achieving thresholdless lasers [27,28]. Additionally, with pioneering effects utilizing the bandgap property of such photonic crystals, many significant applications and relevant optical manipulation can be realized, which are particularly important for the on-demand integration of on-chip light sources [29–32].

On the other hand, due to the formation of standing waves with zero group velocity of light at the band edges in such a photonic band structure, the resonant effect can also be exploited to achieve a large-area coherent resonance for lasing action, enabling a higher power operation while keeping the symmetric beam profile with narrow beam divergence and spectral width. Subsequently, we overview the recent development of such band edge types of photonic crystal lasers.

### 3.1. Operation Principle

The exploitation of band-edge resonance can give rise to a large-area coherent resonance for lasing action; hence, a two-dimensional photonic crystal can be adopted as a laser cavity, generating a lateral cavity photonic-crystal surface-emitting laser. Accordingly, in 1999, two groups independently proposed this concept for the semiconductor lasers embedded with two-dimensional photonic crystals as laser cavities [33,34]. As shown in Figure 5a, M. Imada et al. presented a laser device with a triangular-lattice photonic crystal via bonding fabrication [33]. In the proposed structure, a  $p$ -InP cladding layer and InGaAsP multiple-quantum-well (MQW) layers serve as an active layer, namely the upper wafer A. For another wafer, namely the bottom wafer B, an  $n$ -InP cladding layer is patterned with a triangular-lattice photonic crystal. Finally, via the wafer fusion technique, a bonded PCSEL device can be fabricated, thus embedding the photonic crystal near the active layer. For such a structure, light emission from the active layer is thereby guided by the  $p$ - and  $n$ -cladding layers, videlicet the adjoined photonic crystal, thus achieving a lasing action.

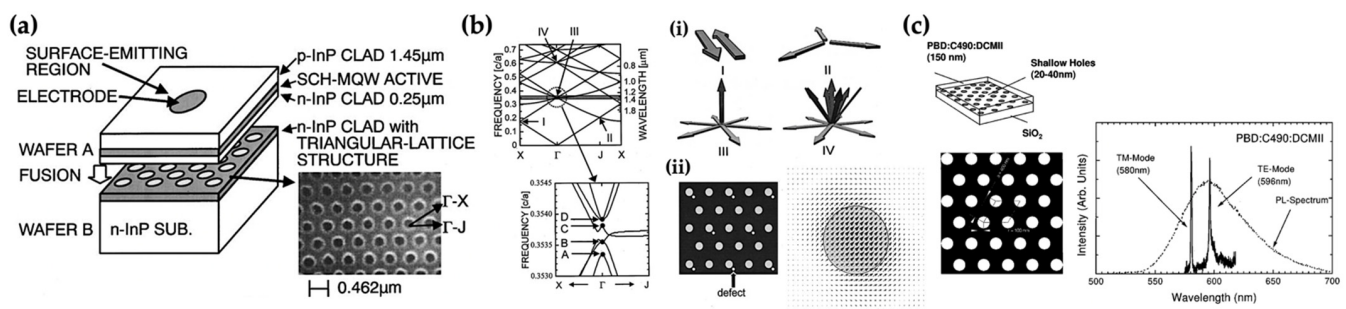


**Figure 5.** (a) Schematic illustration of the surface-emitting laser embedded with a 2D triangular-lattice structure via wafer fusion technique [33]. (b) Band diagram of a 2D photonic crystal [35]. **Insets:** (i) Schematic illustration for the propagating directions of coupled waves at points I–IV. (ii) Schematic illustration of defects introduced into a 2D photonic crystal. The corresponding electric field pattern can be calculated via finite-difference time-domain (FDTD) method. (c) Schematic illustration of layer structure with a two-dimensional triangular lattice and the corresponding emission spectra from the device [34]. Two lasing peaks with different polarizations can be observed. In addition, the spontaneous emission spectrum from the gain medium is shown with a dashed line.

In 2002, relevant lasing modes in a two-dimensional photonic crystal were theoretically and experimentally investigated with an in-plane multidirectional distributed feedback effect, as shown in Figure 5b [35]. Output laser light beam can be manipulated and coupled into specific directions. Moreover, a photonic-crystal laser device adopted with the band-edge mode at  $\Gamma$ -point enables specific radiation in a surface normal direction. Thus, an optimal band edge is figured out for a surface emission laser with truly coherent two-dimensional resonance.

It is worth mentioning that the exploitation of band-edge resonance in a triangular-lattice photonic crystal for lasing action is also demonstrated by M. Meier et al. in 1999, as shown in Figure 5c [34]. However, they did not conduct a further investigation for the achievement of coherent two-dimensional resonance. Multidirectional light propagation is not coupled to the in-plane photonic-crystal lattice structure, and thus two lasing peaks with different polarizations can be observed. A fast and accurate computational technique, namely the plane wave admittance method, for determining the electromagnetic modes

in photonic structures was proposed by M. Dems et al. in 2005 as well [36]. Thereupon, several remarkable efforts, especially for the relevant numerical simulation, are established by M. Dems's group, making great contributions to modeling activities [36–40].

### 3.2. Light-Emitting Control and Emission Wavelength Expansion

For the betterment of laser light emission, namely toward a high-power single-mode operation with controllability, relevant research of PCSELS was thereafter shifted to the photonic crystals with square-lattice structure. For such a square-lattice structure, the corresponding four fundamental Bloch waves, oscillating in transverse-electric (TE) polarization, cannot be directly coupled, yet the use of higher-order Bloch waves can indirectly accomplish [41–45]. However, the employment of higher-order Bloch waves needs a large refractive index contrast; thus, a photonic crystal embedded with air holes is necessary. In addition, the resonance in a photonic crystal with relevant polarization and its coupled-wave analysis is crucial as well [45–50].

Furthermore, the eventual laser light beam pattern, videlicet the far-field beam profile, from a PCSEL device is via multidirectional coupling, radiating laser light in the surface normal direction. The relationship between far-field beam profile and near-field electromagnetic field distribution can be investigated and expressed via Fourier transformation. Thus, this transformation relationship can provide tunability and controllability for the eventual electromagnetic field distribution. By engineering the geometry of the unit cell structure for a photonic crystal, the corresponding electromagnetic field distribution can thereby be modified. Accordingly, in 2001, S. Noda et al. demonstrated the polarization mode selection in a PCSEL via unit cell structure design [44]. A common band diagram of a square-lattice photonic crystal with a circular unit cell is shown in Figure 6a. The formation of standing waves at the band edges in such a photonic band structure can be observed. While changing the geometry of unit cells from circulars to ellipses, significant modification of the corresponding electromagnetic field distribution can be acquired, paving a novel strategy for the exact control of polarization modes, as shown in Figure 6b. With the recent progress of metaphotonics, such a structural modification for PCSEL holds great promise not only for the novel photonic devices manipulating corresponding light emission but also for ultracompact optical devices in simplicity [51].

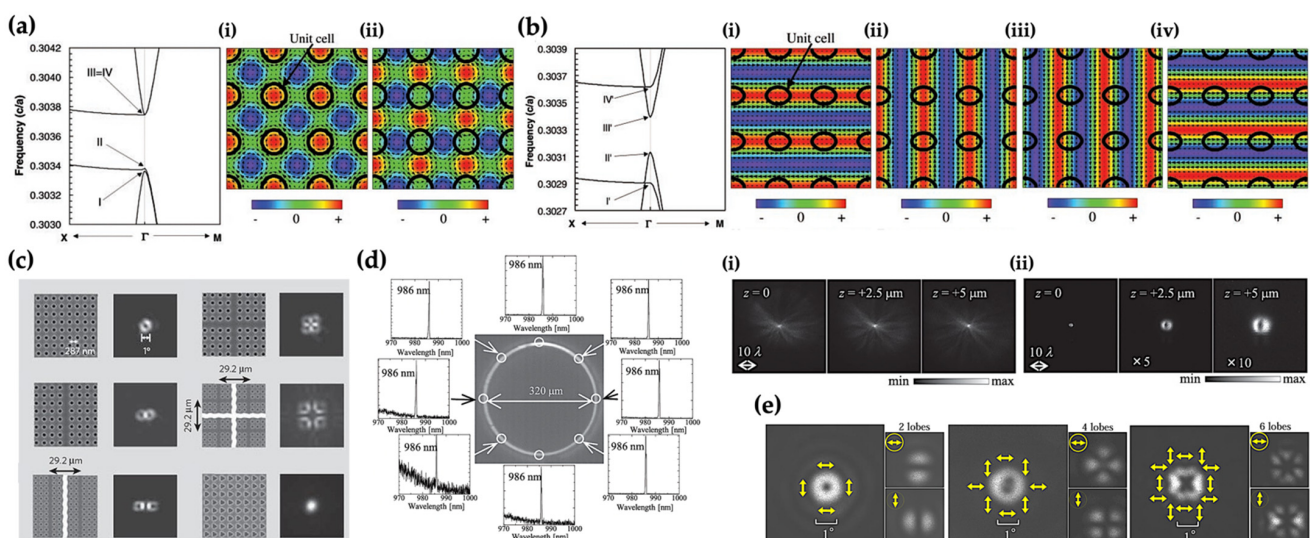


**Figure 6.** (a) Band structure of a 2D photonic crystal structure with square lattice and circular unit cell [44]. **Insets: (i,ii)** The corresponding electromagnetic field distributions at band edges I and II, respectively. Red and blue areas indicate the amplitudes of corresponding magnetic fields in the direction perpendicular to the plane. Arrows and thick black circles indicate the in-plane electric field

vectors and the locations of lattice points, respectively. (b) Band structure of a 2D photonic crystal structure with square lattice and elliptical unit cell [51]. **Insets: (i–iv)** The corresponding electromagnetic field distributions at band edges I to IV. Unified electromagnetic field distributions can be observed at individual band edges. Thus, a linear polarization can be expected. (c) Miscellaneous beam patterns generated by photonic-crystal lasers with engineered lattice points and/or lattice phases [52]. (d) Near-field image and the corresponding spectra distributions of a photonic crystal ring-cavity laser under the pulsed condition at room temperature [53]. **Insets: (i,ii)** Corresponding focusing properties of a radially polarized halo-shaped beam and a radially polarized doughnut-shaped beam, respectively. (e) Versatile doughnut-shaped beam patterns from fabricated devices with photonic crystal structures [54]. Vector beams can be observed with different lobes by the polarizer. Yellow arrows indicate the electric field direction.

In 2006, E. Miyai et al. demonstrated a series of PCSELS with miscellaneous engineered lattice points and/or lattice phases, as shown in Figure 6c [52]. As a result, originating from the asymmetry of lattice points, the symmetrical electric field will be broken while the shape of lattice points is changed to a triangular shape. Consequently, the corresponding surface-emitted beams can exhibit versatile lobe forms, namely diverse beam patterns on-demand, maintaining stable single-mode oscillation.

On the other hand, the geometrical arrangement of a photonic crystal can be another strategy. In 2012, K. Kitamura et al. presented a needle-like focus from a photonic-crystal ring-cavity laser, as shown in Figure 6d [53]. By properly manipulating the inner and outer radii of ring photonic crystal, the proposed ring-cavity laser can emit halo laser light beams with radial polarization. In addition, such a laser light emission exhibits a needle-like focus, and the corresponding spot size can shrink down to 0.4 times its wavelength with an evaluated depth of focus (DoF) longer than 10 times its wavelength for an objective lens of 0.9 numerical aperture (NA). In 2011, S. Iwahashi et al. successfully generated doughnut-shaped vector laser light beams, manifesting versatile higher-order polarization states from PCSELS with designed lattice structures, as shown in Figure 6e [54]. Moreover, a systematic analysis of the generated vector beams is conducted through the polarizer, paving a deeper understanding of the cavity symmetry of PCSELS and the consequent effects.

With the advancements for autonomous vehicles, i.e., self-driving cars, relevant methods regarding depth perception and LiDAR application are prosperously developed. The expeditious needs for miniature devices with multi functionalities are in urgent demand. For laser light scanning in LiDAR application, the aforesaid strategy with an engineered geometry of unit cell structure can be a practical solution for the monolithic integration to achieve an on-chip modification of electromagnetic field distribution. Consequently, a reliable technique for beam steering is developed, assembling an array of PCSELS [55]. Each PCSEL in this array can be electronically driven, thus rapidly emitting laser light beams in distinct directions.

In 2010, Y. Kurosaka et al. demonstrated PCSELS with on-chip controllability of the beam direction, as shown in Figure 7a [55]. Based on the pioneer efforts, the corresponding output laser light beam from PCSELS can be determined by the resonant condition, and thus a properly engineered geometry of the unit cell structure in a photonic crystal is crucial [44,51–54,56,57]. Therefore, they proposed relevant artificial lasing band edges with a photonic-crystal structure composed of both square and rectangular lattices. By manipulating relative lattice constants, the corresponding laser light emission in such a PCSEL device with composite photonic-crystal structures can achieve on-chip controllability in a range of directions. It is worth mentioning that beam steering via resonance detuning is proposed by M. T. Johnson et al. in 2013 [58]. Surface etched photonic crystals on VCSEL array elements are employed for investigating the dynamic coupled-mode theory. Thus, a complete theoretical connection between injected currents and the beam steering direction is established. Accordingly, several surface etched photonic crystals on laser devices are demonstrated by K. D. Choquette's group, paving interesting insights into miscellaneous responses and relevant manipulation of laser devices with photonic-crystal structures [58–65].

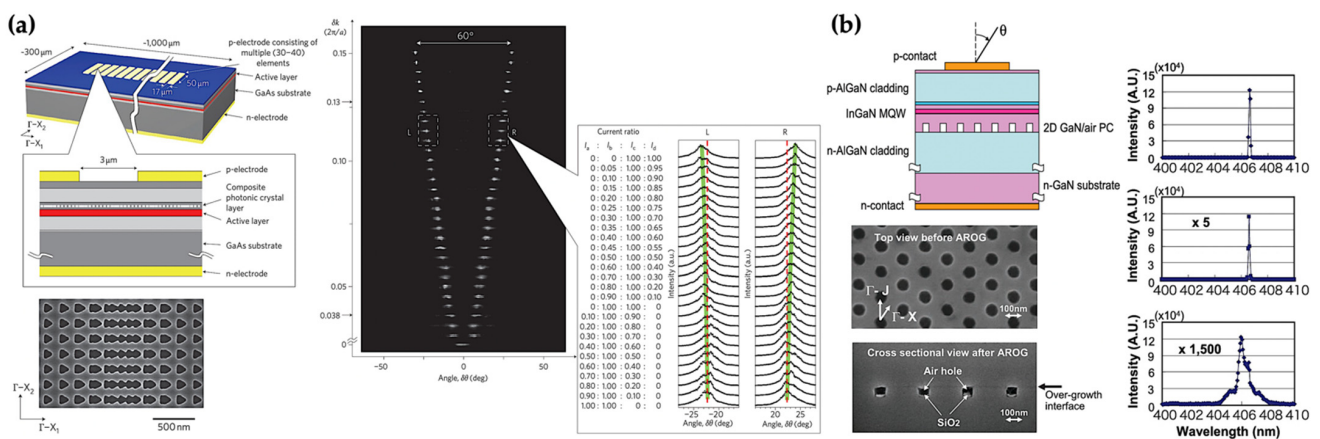


**Figure 7.** (a) Schematic illustration of device structure and the corresponding on-chip beam-steering functionality [55]. The bottom left side of scanning electron microscope (SEM) image shows a portion of fabricated composite photonic crystal with the square and rectangular lattice structures. (b) Schematic illustration of the GaN-based photonic-crystal laser device and the corresponding emission spectra above the current threshold [66]. The bottom left side of SEM images show the top view and the cross-sectional view before and after the fabrication of air holes retained overgrowth, respectively. As a result, the well-defined GaN/air periodic structure inside the GaN epitaxial layer can be observed.

On the one hand, extending the lasing wavelength range provides a capacious application field [66–68]. In 2008, H. Matsubara et al. proposed a GaN-based PCSEL, emitting laser light beams in the blue-violet regime, as shown in Figure 7b [66]. To construct a two-dimensional GaN/air photonic-crystal structure, a new fabrication called air holes retained overgrowth is developed, exploiting the particular characteristics of GaN growth. Meanwhile, this new fabrication can prevent the use of the aforesaid wafer fusion technique and the complicated etching techniques in a GaN system [33,69,70]. Consequently, a current-driven PCSEL with a laser light emission at 406.5 nm was successfully created. Moreover, considering a high-power PCSEL operation with narrow beam divergence, the mastery of band-edge resonance along with engineering the geometry of the unit cell structure is crucial [71–76]. Relevant effects during the growth of photonic-crystal air holes are profoundly investigated by T. C. Lu’s group [71,76].

### 3.3. High-Power Operation with the Concept of Double-Lattice Structure

The mastery of band-edge resonance along with engineering the geometry of unit cell structure for a PCSEL provides not only the corresponding light-emitting controllability but also a crucial part in the high-power operation with narrow beam divergence. To achieve a high-power operation, an air-hole-retained regrowth method is thereby developed, preventing the interface of discontinuous crystallinity while using the aforesaid wafer fusion technique [33,77]. Regarding engineering the geometry of unit cell structure, an asymmetric lattice-point shape is hence exploited, namely a square-lattice photonic crystal with right-angled triangular lattice points. Moreover, a regrowth method for epitaxy to bury the etched structure is also investigated to improve the stability of lasing oscillation, generating a lower refractive index contrast at the interface [78]. It is worth mentioning that a 0.2 W class PCSEL device that revolved around these engineered photonic crystals has been commercially available since 2013 [79].

In 2014, K. Hirose et al. demonstrated a watt-class PCSEL, as shown in Figure 8a [80]. For such a PCSEL structure, the cladding layer, MQW layers, and blocking layer are grown in sequence. Next, a *p*-GaAs layer is grown for preparing photonic crystals on an *n*-GaAs substrate. The corresponding lattice constant of fabricated square-lattice photonic crystal with right-angled triangular lattice points is exactly aligned with the band-edge mode at  $\Gamma$ -point, emitting light from MQW layers at an accurate wavelength. Finally, the *p*-type

cladding layer and contact layer are directly grown on the as-prepared photonic crystal patterns via the air-hole-retained regrowth method based on metal–organic vapor phase epitaxy (MOVPE). Such a regrowth method exploits the innate difference in growth rates depending on distinct crystalline facets. As a result, the burial air holes can be retained near the active layer. Moreover, to obtain a high-power operation, a sufficient extraction for output light emission is necessary. Thus, the asymmetric lattice-point shapes, namely the right-angled triangular lattice points, herein are also employed to break the symmetrical electric field, increasing the surface-emitted beams. Consequently, with these efforts, such a PCSEL exhibits a watt-class laser light emission, up to 1.5 W output power. While operating with an output power of 0.5 W, the overall divergence angle is less than  $0.5^\circ$ , suggesting a marvelous beam quality.

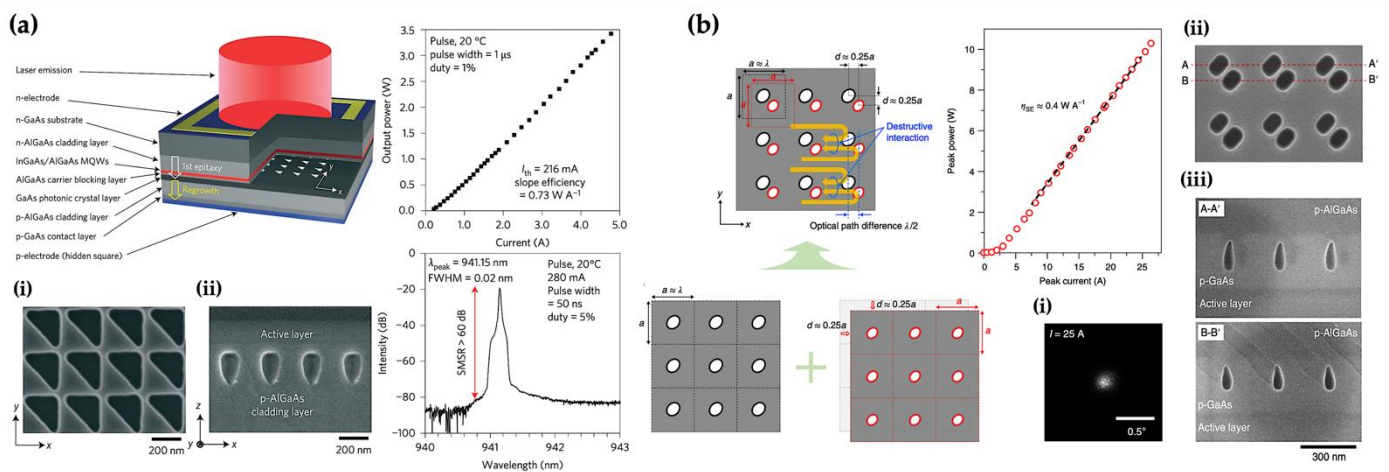


**Figure 8.** (a) Schematic illustration of device structure and the corresponding lasing characteristics operated under room temperature pulsed conditions [77]. A watt-class laser light emission with high beam quality can be achieved with such a photonic-crystal laser device. **Insets:** (i,ii) The SEM images show the top view and the cross-sectional view before and after the burial by metal–organic chemical vapor deposition (MOCVD) regrowth, respectively. After burial, well-defined photonic-crystal air holes can be observed. (b) Schematic illustration for the concept of a double-lattice photonic crystal and the corresponding lasing characteristic operated under room-temperature pulsed conditions [45]. With the adoption of such double-lattice photonic-crystal structure, remarkable 10-watt-class laser light emission with quite narrow beam divergence can be attained. **Insets:** (i) Measured far-field pattern for such a laser device operated with an injection current of 25 A. A quite narrow divergence angle of less than  $0.3^\circ$  can be observed. (ii,iii) The SEM images show the top view and the cross-sectional view before and after the MOVPE regrowth technique, respectively.

To further attain a high-power operation, namely toward a 10-watt-class laser light emission, the lasing area in a photonic crystal should be expanded, obtaining enough gain for light amplification. Holding a selective lasing oscillation in fundamental mode is vital for a high-power laser light emission. However, with the existence of sufficient field intensity around the photonic-crystal edge, a multimodal lasing oscillation usually occurs while enlarging the photonic-crystal area. Moreover, due to the shrinkage of threshold gain margin with an enlarged lasing area, namely an implicit threshold difference among the fundamental mode and higher-order modes, the multimodal lasing oscillation thereby is inevitable in an expanded conventional photonic crystal. Subsequently, the concept of the double-lattice structure emerges to roll with the punches [45,80,81].

Thus, in 2019, M. Yoshida et al. proposed a modified photonic crystal with the concept of double-lattice structure to overcome this challenge, as shown in Figure 8b [45]. For such a modified photonic crystal, the double-lattice structure can provide a proper optical path difference between the backward diffracted light beams with a phase difference of  $180^\circ$ , thus destructively interfering with these in-plane light beams. Therefore, relevant optical modes

spread out, and the lasing area can be expanded. Moreover, this expanded lasing area can maintain a widened threshold gain margin as well, leading to the suppressed higher-order modes. In the proposed modified photonic crystal, the corresponding resonator area is even increased up to  $500 \mu\text{m}^2$ . A remarkable 10-watt-class laser light emission with quite a narrow beam divergence can be attained. The asymmetry of lattice points can be adopted as well, paving a further optimization. In addition to the double-lattice structure, the use of topology can be another novel way to manipulate relevant properties inside the cavity [82–84].

Furthermore, in 2021, M. Yoshida et al. considered a PCSEL with the backside reflection of distributed Bragg reflector (DBR) mirror, increasing the corresponding extraction and efficiency for output light emission [85]. As a result, a 10-watt-class laser light emission can be acquired with an extraordinary beam divergence of  $0.17^\circ$  (the  $1/e^2$  beam width) and  $0.1^\circ$  (the full width at half maximum, FWHM). In other words, nearly diffraction-limited beam divergence is achieved in such a  $500 \mu\text{m}^2$  resonator area.

#### 4. Toward a Lens-Free and Adjustment-Free ToF LiDAR System

As the tendency of miniaturization in relevant optical technologies, ultracompact optical devices with miscellaneous functionalities are urgently needed. With the state-of-the-art progress in PCSELS, such laser devices can provide higher-power and extraordinarily narrow-divergence laser light beams while keeping a symmetric beam profile. Therefore, based on these laser devices, prospects to ameliorate the bulky form factor of common optical devices are in demand.

Owing to the blossom of advancements for autonomous vehicles, i.e., self-driving cars, depth perception, and LiDAR applications are flourishing. In addition, for a ToF LiDAR system, PCSELS can be appropriate laser light sources as well. In 2021, M. Yoshida et al. proposed a 10-watt-class PCSEL with DBR, operating in pulsed mode with the repetition rate and corresponding pulse width of 1 kHz and 100 ns, respectively [85]. Moreover, in 2021, R. Morita et al. introduced the design of two-dimensionally arranged gain and loss sections, and the corresponding operation in pulsed mode can even reach astonishing results [86]. In such a well-designed PCSEL, a relevant peak power of 20 W can be achieved with the repetition rate and corresponding pulse width of 1 GHz and 35 ps, respectively.

Additionally, the performance trade-offs of PCSEL technology emerge with several challenges in power scaling, modal competition, charge injection control, etc. Auspiciously, with abundant efforts, these challenges can be ameliorated and conquered [15]. For real-world applications, the thermal characteristics and relevant management of laser devices are crucial and should be concerned as well [87–92]. In 2020, M. De Zoysa et al. conducted the relevant thermal analysis for PCSELS under continuous wave (CW) operation with heat dissipation [92]. The corresponding temperature properties for an assembled double-lattice PCSEL in a water-cooling package with a highly thermally conductive sub-mount are investigated, providing a practical paradigm for high-power operation. Nowadays, artificial intelligence-assisted technology can be even adopted for the fabrication as well [93]. Thus, as shown in Figure 9, these demonstrated paradigms can promise pavements toward a lens-free and adjustment-free ultracompact ToF LiDAR system soon.

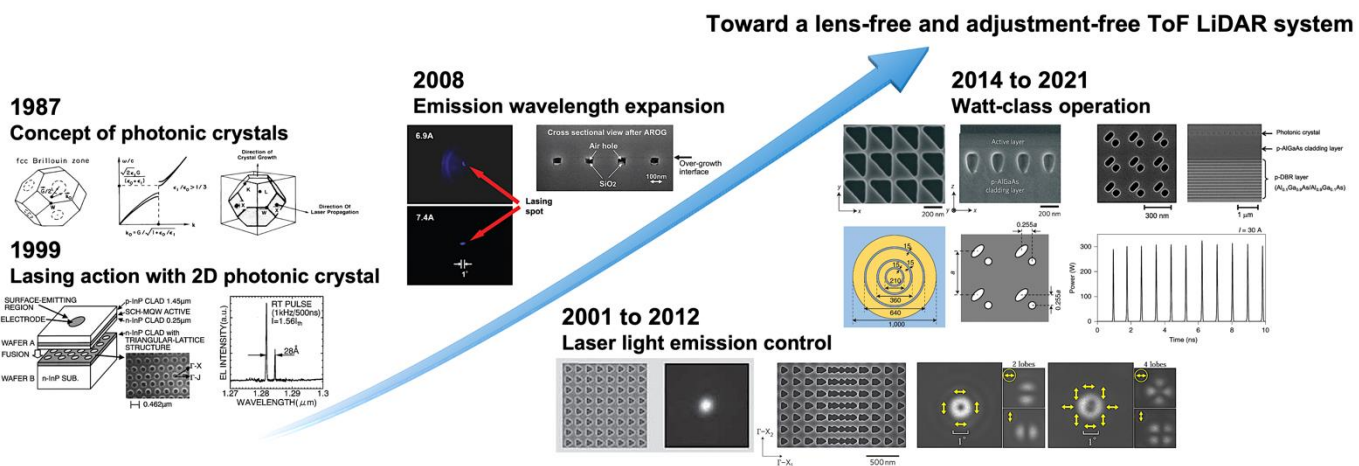


**Figure 9.** Development progress of PCSEL technology toward an ultracompact ToF LiDAR system [21,22,33,34,45,52,54,55,66,77,86].

**4.1. Benchmark of PCSELS for ToF LiDAR System**

Herein, the remarkable development progress of aforesaid PCSELS is outlined. The relevant benchmark for a ToF LiDAR system is compared in Table 1.

**Table 1.** Benchmark of PCSELS for a ToF LiDAR system (designed wavelength = 940 nm).

Year	2014 [77]	2019 [45]	2021 [85]	2021 [86]
Lattice	Square lattice Isosceles right triangle	Square lattice Double hole	Square lattice Double hole	Square lattice Double hole
Structure (µm)	<i>n</i> -side up, 200	<i>n</i> -side up, 500	<i>n</i> -side up, 500	<i>n</i> -side up, 400 or 1000
Extra design	NA	NA	w/ <i>p</i> -side DBR	w/loss section
Operation mode	<b>Pulsed mode @20 °C</b> pulse width = 1 µs, duty cycle = 1%	<b>Pulsed mode</b> @200 Hz, pulse width = 200 ns	<b>Pulsed mode</b> @1 kHz, pulse width 100 ns	<b>Pulsed mode</b> @1.1 GHz, pulse width ~ 35 ps
	CW mode @20 °C	CW mode @5–20 °C		
Threshold current (A)	0.216 0.22	2 3.3	2.1	NA
Slope efficiency (W/A)	0.73 0.66	0.4 0.48	0.8	NA
Maximum power (W)	<b>3.4 @5 A</b> <b>(limited by driver)</b> 1.5 @2.5 A	<b>&gt;10 @25 A</b> 7	<b>&gt;10 @15 A</b>	<b>20 @3–4 A @1 GHz,</b> <b>pulse width ~ 35 ps</b> <b>300 @30 A @1 GHz,</b> <b>pulse width ~ 40 ps</b>
Divergence angle	<b>&lt;1°</b> <3° @1.5 W	<b>&lt;0.3° @10 W</b> NA	<b>0.17° @10 W</b> NA	<b>0.35°</b> NA

The significance of bold indicates relevant figure of merits (FoMs) for a ToF LiDAR system.

**4.2. Real-Time Simulation and Visualisation via HELIOS**

To gain a better insight into the factor of beam divergence for a LiDAR system, a systematic simulation is thereby conducted via the Heidelberg LiDAR Operations Simulator (HELIOS), providing real-time visualization of relevant point cloud results [94]. The simulation is set based on a practical LiDAR system incorporated with the micro-electro-mechanical-system (MEMS) mirror scanner and a single-photon imager, referring to the pioneering works presented by M. Yoshida et al. in 2013 [95]. The scene involves three cars. Car 1, Car 2, and Car 3 are placed in locations of 10 m, 17 m, and 28 m, respectively. In addition, a pedestrian in the location of 12 m got stuck in traffic.

The laser light source with an average power of 96 mW is adopted in the simulation. In such a system, the pulse repetition frequency and pulse width are set as 600 kHz and 4 ns, respectively. For the attenuation terms, the atmospheric visibility is set as 23 km. In addition, for the relevant mechanical configurations, a scanning frequency of 1.4 kHz is set with the field of view (FoV) for the overall sensor of  $45^\circ$  by  $11^\circ$ .

For a LiDAR system, beam divergence plays an important role in preserving sufficient power density for ranging. An ideal Gaussian laser light beam will propagate and spread out, depending on the divergence angle [96]. Thus, a laser light beam with a larger beam divergence will result in the dilution of power density, limiting the working distance. Moreover, a larger beam divergence will inevitably generate bigger footprints on the objects, decreasing the resolution of detection. Hereupon, a series of simulation studies varying the beam divergence of  $2^\circ$ ,  $1^\circ$ ,  $0.5^\circ$ , and  $0.2^\circ$  are conducted, providing the corresponding intensity and depth images, as shown in Figures 10a and 10b, respectively. With a divergence angle of  $2^\circ$ , relevant intensity and depth images are both blurred. The pedestrian is buried and hard to identify in both intensity and depth images. Auspiciously, the narrower divergence angles the clearer images. As the divergence angle shrinks down to  $0.5^\circ$ , clear contours can be identified. Moreover, a shadow of a pedestrian emerges, and the relevant details of Car 1's rear wheel can be observed as well. While the divergence angle is down to  $0.2^\circ$ , the contours of the pedestrian's shadow and even of Car 1's taillight can be identified. Through this intuitive real-time visualization of relevant point cloud results, the effects of beam divergence are very significant for the LiDAR system.

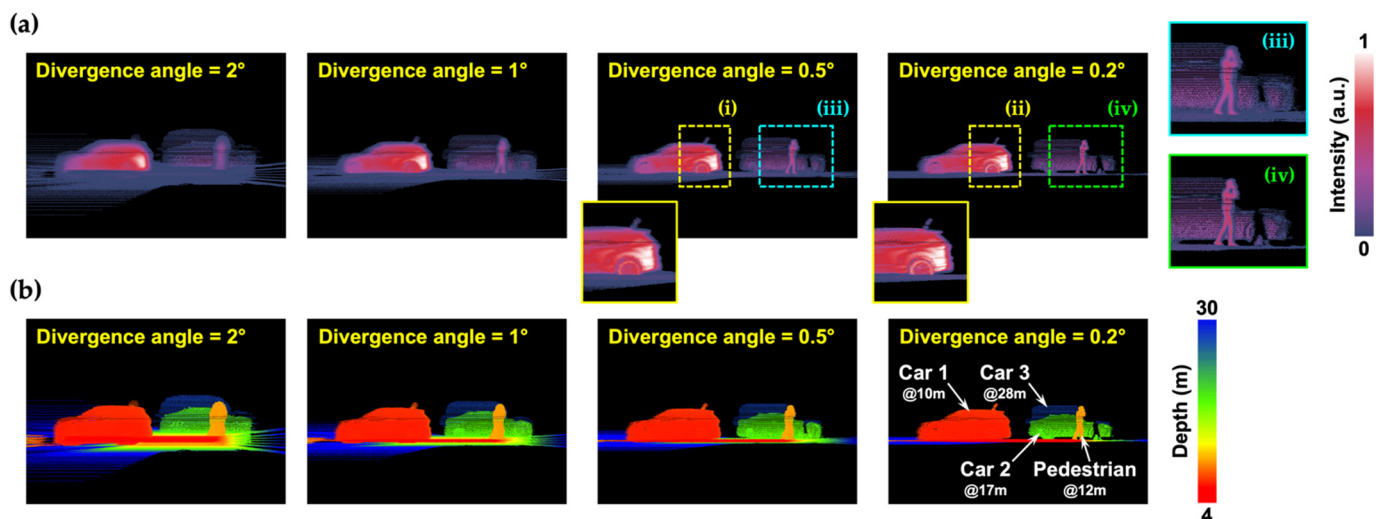


**Figure 10.** Simulated point cloud results of (a) scalar field intensity and (b) corresponding depth perception. **Insets of (a):** Some zoom-in details observed in the result of scalar field intensity. (i,ii) As the beam divergence angle is shrunk down to  $0.2^\circ$ , relevant details of rear tire, wheel disk, and even the taillight of Car 1 can be identified. (iii,iv) The narrower beam divergence, the clearer the pedestrian's contour. Meanwhile, a pedestrian's shadow can be observed, emerging on Car 2.

## 5. Conclusions

The comprehensive analyses of PCSEL-relevant scientific publications and patent documents are conducted. Along with the progress of PCSEL technology development, we thereby review this revolutionary semiconductor laser technology. With the blossom of PCSEL-relevant annual patent counts in 2015, a tendency for the practical uses of PCSEL can be observed. PCSEL can provide not only a symmetric beam profile with narrow beam divergence but also the tunability and controllability for the eventual electromagnetic field distribution, videlicet the far-field beam profile. In addition, while the concept of double-lattice photonic-crystal structure is introduced, a high-power single-mode operation, up to ten- or even hundred-watt class, can be achieved. Considering the design of two-dimensionally arranged gain and loss sections, PCSEL can operate in a pulsed mode,

with a pulse repetition frequency and a pulse width of 1.1 GHz and 35 ps, respectively [86]. Furthermore, real-time visualization of relevant point cloud results varying the beam divergence is conducted via the HELIOS, providing an intuitive way to confirm the relevant final effects. Thus, owing to PCSEL technology with these marvelous advantages, a paradigm shift in LiDAR application is ongoing. The prospects to ameliorate the bulky form factor of a LiDAR system and toward a lens-free and adjustment-free ultracompact apparatus in simplicity can be expected.

**Author Contributions:** Conceptualization, S.-C.C. and H.-C.K.; investigation, Y.-H.H., C.L., W.-C.M., W.-C.H. and K.-B.H.; data curation, C.L.; writing—original draft preparation, Y.-H.H. and C.L.; writing—review and editing, Y.-H.H., C.-L.L., C.L., S.-C.C. and H.-C.K.; supervision, H.-C.K.; project administration, S.-C.C. All authors have read and agreed to the published version of the manuscript.

**Funding:** This research was funded by the Ministry of Science and Technology in Taiwan (Grant Nos. MOST 110-2622-8-A49-008-SB).

**Institutional Review Board Statement:** Not applicable.

**Informed Consent Statement:** Not applicable.

**Data Availability Statement:** Not applicable.

**Acknowledgments:** The authors would like to gratefully acknowledge Tien-Chang Lu at National Yang Ming Chiao Tung University for the fruitful discussion.

**Conflicts of Interest:** The authors declare no conflict of interest.

## References

1. 3D Imaging and Sensing-Technology and Market Trends 2021. Available online: <https://www.i-micronews.com/products/3d-imaging-and-sensing-technology-and-market-trends-2021/> (accessed on 24 April 2022).
2. Light Detection and Ranging (LiDAR) Market. Available online: <https://www.fortunebusinessinsights.com/light-detection-and-ranging-lidar-market-101969> (accessed on 24 April 2022).
3. Iga, K. Laboratory Notebook. March 1977.
4. Iga, K.; Koyama, F.; Kinoshita, S. Surface emitting semiconductor lasers. *IEEE J. Quantum Electron.* **1988**, *24*, 1845–1855. [CrossRef]
5. Iga, K. Surface-emitting laser-its birth and generation of new optoelectronics field. *IEEE J. Sel. Top. Quantum Electron.* **2000**, *6*, 1201–1215. [CrossRef]
6. Iga, K. Vertical-cavity surface-emitting laser: Its conception and evolution. *Jpn. J. Appl. Phys.* **2008**, *47*, 1. [CrossRef]
7. Iga, K. Vertical-cavity surface-emitting laser (VCSEL). *Proc. IEEE* **2013**, *101*, 2229–2233. [CrossRef]
8. Koyama, F.; Kinoshita, S.; Iga, K. Room temperature cw operation of GaAs vertical cavity surface emitting laser. *IEICE Trans. Electron.* **1988**, *71*, 1089–1090.
9. Larsson, A. Advances in VCSELs for communication and sensing. *IEEE J. Sel. Top. Quantum Electron.* **2011**, *17*, 1552–1567. [CrossRef]
10. Moser, P.; Lott, J.A.; Bimberg, D. Energy efficiency of directly modulated oxide-confined high bit rate 850-nm VCSELs for optical interconnects. *IEEE J. Sel. Top. Quantum Electron.* **2013**, *19*, 1702212. [CrossRef]
11. Pruijboom, A.; Apetz, R.; Conrads, R.; Deppe, C.; Derra, G.; Gronenborn, S.; Gu, X.; Kolb, J.S.; Miller, M.; Moench, H.; et al. VCSEL arrays expanding the range of high-power laser systems and applications. *J. Laser Appl.* **2016**, *28*, 032005. [CrossRef]
12. Ebeling, K.J.; Michalzik, R.; Moench, H. Vertical-cavity surface-emitting laser technology applications with focus on sensors and three-dimensional imaging. *Jpn. J. Appl. Phys.* **2018**, *57*, 08PA02. [CrossRef]
13. Liu, A.; Wolf, P.; Lott, J.A.; Bimberg, D. Vertical-cavity surface-emitting lasers for data communication and sensing. *Photonics Res.* **2019**, *7*, 121–136. [CrossRef]
14. Ishizaki, K.; De Zoysa, M.; Noda, S. Progress in photonic-crystal surface-emitting lasers. *Photonics* **2019**, *6*, 96. [CrossRef]
15. Kalapala, A.; Song, A.; Pan, M.; Gautam, C.; Overman, L.; Reilly, K.; Rotter, T.; Balakrishnan, G.; Gibson, R.; Bedford, R.; et al. Scaling challenges in high power photonic crystal surface-emitting lasers. *IEEE J. Quantum Electron.* **2022**. [CrossRef]
16. Wang, Z.; Tong, C.; Wang, L.; Lu, H.; Tian, S.; Wang, L. Photonic crystal surface emitting laser operating in pulse-periodic regime with ultralow divergence angle. *Photonics* **2021**, *8*, 323. [CrossRef]
17. Taylor, R.J.; Childs, D.; Hogg, R. Vector photonics: The commercial journey of PCSELs and their pathway to high power. In Proceedings of the SPIE High-Power Diode Laser Technology XX, San Francisco, CA, USA, 22 January–28 February 2022; Volume PC1198304.
18. de Zoysa, M.; Inoue, T.; Yoshida, M.; Ishizaki, K.; Kunishi, W.; Gellera, J.; Noda, S. Light detection functionality of photonic-crystal lasers. *IEEE J. Quantum Electron.* **2021**, *57*, 6400208. [CrossRef]

19. Noda, S. Progress of photonic crystal surface-emitting lasers: Paradigm shift for lidar sensing and laser processing. In Proceedings of the Laser Resonators, Microresonators, and Beam Control XXIII, Virtual, 6–12 March 2021; Volume 11672, p. 1167203.
20. Noda, S. Photonic crystal surface-emitting lasers and their application to lidar. In Proceedings of the 2021 26th Microoptics Conference (MOC), Hamamatsu, Japan, 26–29 September 2021; pp. 1–2.
21. Yablonovitch, E. Inhibited spontaneous emission in solid-state physics and electronics. *Phys. Rev. Lett.* **1987**, *58*, 2059. [[CrossRef](#)]
22. John, S. Strong localization of photons in certain disordered dielectric superlattices. *Phys. Rev. Lett.* **1987**, *58*, 2486. [[CrossRef](#)]
23. Web of Science (WoS) Bibliometric Database. Available online: [www.webofscience.com](http://www.webofscience.com) (accessed on 27 April 2022).
24. Derwent Innovation's Patent Database. Available online: [www.derwentinnovation.com](http://www.derwentinnovation.com) (accessed on 27 April 2022).
25. Purcell, E.M. Spontaneous emission probabilities at radio frequencies. *Phys. Rev.* **1946**, *69*, 681.
26. Heinzen, D.J.; Childs, J.J.; Thomas, J.E.; Feld, M.S. Enhanced and inhibited visible spontaneous emission by atoms in a confocal resonator. *Phys. Rev. Lett.* **1987**, *58*, 1320. [[CrossRef](#)]
27. Hirayama, H.; Hamano, T.; Aoyagi, Y. Novel surface emitting laser diode using photonic band-gap crystal cavity. *Appl. Phys. Lett.* **1996**, *69*, 791–793. [[CrossRef](#)]
28. Tandraechanurat, A.; Ishida, S.; Guimard, D.; Nomura, M.; Iwamoto, S.; Arakawa, Y. Lasing oscillation in a three-dimensional photonic crystal nanocavity with a complete bandgap. *Nat. Photonics* **2011**, *5*, 91–94. [[CrossRef](#)]
29. Ryu, H.Y.; Notomi, M.; Lee, Y.H. High-quality-factor and small-mode-volume hexapole modes in photonic-crystal-slab nanocavities. *Appl. Phys. Lett.* **2003**, *83*, 4294–4296. [[CrossRef](#)]
30. Takano, H.; Akahane, Y.; Asano, T.; Noda, S. In-plane-type channel drop filter in a two-dimensional photonic crystal slab. *Appl. Phys. Lett.* **2004**, *84*, 2226–2228. [[CrossRef](#)]
31. Sugitatsu, A.; Asano, T.; Noda, S. Line-defect-waveguide laser integrated with a point defect in a two-dimensional photonic crystal slab. *Appl. Phys. Lett.* **2005**, *86*, 171106. [[CrossRef](#)]
32. Nozaki, K.; Kita, S.; Baba, T. Room temperature continuous wave operation and controlled spontaneous emission in ultrasmall photonic crystal nanolaser. *Opt. Express* **2007**, *15*, 7506–7514. [[CrossRef](#)]
33. Imada, M.; Noda, S.; Chutinan, A.; Tokuda, T.; Murata, M.; Sasaki, G. Coherent two-dimensional lasing action in surface-emitting laser with triangular-lattice photonic crystal structure. *Appl. Phys. Lett.* **1999**, *75*, 316–318. [[CrossRef](#)]
34. Meier, M.; Mekis, A.; Dodabalapur, A.; Timko, A.; Slusher, R.E.; Joannopoulos, J.D.; Nalamasu, O. Laser action from two-dimensional distributed feedback in photonic crystals. *Appl. Phys. Lett.* **1999**, *74*, 7–9. [[CrossRef](#)]
35. Imada, M.; Chutinan, A.; Noda, S.; Mochizuki, M. Multidirectionally distributed feedback photonic crystal lasers. *Phys. Rev. B* **2002**, *65*, 195306. [[CrossRef](#)]
36. Dems, M.; Kotynski, R.; Panajotov, K. Planewave admittance method—A novel approach for determining the electromagnetic modes in photonic structures. *Opt. Express* **2005**, *13*, 3196–3207. [[CrossRef](#)] [[PubMed](#)]
37. Drong, M.; Dems, M.; Perina, J.; Fordos, T.; Jaffres, H.Y.; Postava, K.; Drouhin, H.J. Time-dependent laser cavity perturbation theory: Exploring future nano-structured photonic devices in semi-analytic way. *J. Lightwave Technol.* **2022**. [[CrossRef](#)]
38. Dems, M. Convergence analysis of various factorization rules in the Fourier-Bessel basis for solving Maxwell equations using modal methods. *Opt. Express* **2021**, *29*, 4378–4391. [[CrossRef](#)] [[PubMed](#)]
39. Frasunkiewicz, L.; Panajotov, K.; Thienpont, H.; Dems, M.; Czynszowski, T. Transverse mode mixing in a coupled-cavity VCSEL. *J. Lightwave Technol.* **2020**, *38*, 5774–5782. [[CrossRef](#)]
40. Kuc, M.; Piskorski, Ł.; Dems, M.; Wasiak, M.; Sokół, A.K.; Sarzała, R.P.; Czynszowski, T. Numerical investigation of the impact of ITO, AlInN, plasmonic GaN and top gold metalization on semipolar green EELs. *Materials* **2020**, *13*, 1444. [[CrossRef](#)]
41. Noda, S.; Kitamura, K.; Okino, T.; Yasuda, D.; Tanaka, Y. Photonic-crystal surface-emitting lasers: Review and introduction of modulated-photonic crystals. *IEEE J. Sel. Top. Quantum Electron.* **2017**, *23*, 1. [[CrossRef](#)]
42. Sakai, K.; Miyai, E.; Noda, S. Coupled-wave model for square-lattice two-dimensional photonic crystal with transverse-electric-like mode. *Appl. Phys. Lett.* **2006**, *89*, 021101. [[CrossRef](#)]
43. Sakai, K.; Miyai, E.; Noda, S. Coupled-wave theory for square-lattice photonic crystal lasers with TE polarization. *IEEE J. Quantum Electron.* **2010**, *46*, 788–795. [[CrossRef](#)]
44. Liang, Y.; Peng, C.; Sakai, K.; Iwahashi, S.; Noda, S. Three-dimensional coupled-wave model for square-lattice photonic crystal lasers with transverse electric polarization: A general approach. *Phys. Rev. B* **2011**, *84*, 195119. [[CrossRef](#)]
45. Yoshida, M.; De Zoysa, M.; Ishizaki, K.; Tanaka, Y.; Kawasaki, M.; Hatsuda, R.; Song, B.; Gellera, J.; Noda, S. Double-lattice photonic-crystal resonators enabling high-brightness semiconductor lasers with symmetric narrow-divergence beams. *Nat. Mater.* **2019**, *18*, 121–128. [[CrossRef](#)] [[PubMed](#)]
46. Koba, M.; Szczepeński, P. Analysis of mode competition in a 2-D square lattice photonic crystal laser with transverse magnetic polarization. *IEEE J. Quantum Electron.* **2015**, *51*, 1–13. [[CrossRef](#)]
47. Yang, Y.; Peng, C.; Liang, Y.; Li, Z.; Noda, S. Three-dimensional coupled-wave theory for the guided mode resonance in photonic crystal slabs: TM-like polarization. *Opt. Lett.* **2014**, *39*, 4498–4501. [[CrossRef](#)] [[PubMed](#)]
48. Yang, Y.; Peng, C.; Li, Z. Semi-analytical approach for guided mode resonance in high-index-contrast photonic crystal slab: TE polarization. *Opt. Express* **2013**, *21*, 20588–20600. [[CrossRef](#)]
49. Liang, Y.; Peng, C.; Ishizaki, K.; Iwahashi, S.; Sakai, K.; Tanaka, Y.; Kitamura, K.; Noda, S. Three-dimensional coupled-wave analysis for triangular-lattice photonic-crystal surface-emitting lasers with transverse-electric polarization. *Opt. Express* **2013**, *21*, 565–580. [[CrossRef](#)] [[PubMed](#)]

50. Noda, S.; Yokoyama, M.; Imada, M.; Chutinan, A.; Mochizuki, M. Polarization mode control of two-dimensional photonic crystal laser by unit cell structure design. *Science* **2001**, *293*, 1123–1125. [[CrossRef](#)] [[PubMed](#)]
51. Hong, Y.H.; Hsu, W.C.; Tsai, W.C.; Huang, Y.W.; Chen, S.C.; Kuo, H.C. Ultracompact nanophotonics: Light emission and manipulation with metasurfaces. *Nanoscale Res. Lett.* **2022**, *17*, 41. [[CrossRef](#)] [[PubMed](#)]
52. Miyai, E.; Sakai, K.; Okano, T.; Kunishi, W.; Ohnishi, D.; Noda, S. Lasers producing tailored beams. *Nature* **2006**, *441*, 946. [[CrossRef](#)] [[PubMed](#)]
53. Kitamura, K.; Nishimoto, M.; Sakai, K.; Noda, S. Needle-like focus generation by radially polarized halo beams emitted by photonic-crystal ring-cavity laser. *Appl. Phys. Lett.* **2012**, *101*, 221103. [[CrossRef](#)]
54. Iwahashi, S.; Kurosaka, Y.; Sakai, K.; Kitamura, K.; Takayama, N.; Noda, S. Higher-order vector beams produced by photonic-crystal lasers. *Opt. Express* **2011**, *19*, 11963–11968. [[CrossRef](#)] [[PubMed](#)]
55. Kurosaka, Y.; Iwahashi, S.; Liang, Y.; Sakai, K.; Miyai, E.; Kunishi, W.; Ohnishi, D.; Noda, S. On-chip beam-steering photonic-crystal lasers. *Nat. Photonics* **2010**, *4*, 447–450. [[CrossRef](#)]
56. Ohnishi, D.; Okano, T.; Imada, M.; Noda, S. Room temperature continuous wave operation of a surface-emitting two-dimensional photonic crystal diode laser. *Opt. Express* **2004**, *12*, 1562–1568. [[CrossRef](#)]
57. Kim, M.; Kim, C.S.; Bewley, W.W.; Lindle, J.R.; Canedy, C.L.; Vurgaftman, I.; Meyer, J.R. Surface-emitting photonic-crystal distributed-feedback laser for the midinfrared. *Appl. Phys. Lett.* **2006**, *88*, 191105. [[CrossRef](#)]
58. Johnson, M.T.; Siriani, D.F.; Peun, T.M.; Choquette, K.D. Beam steering via resonance detuning in coherently coupled vertical cavity laser arrays. *Appl. Phys. Lett.* **2013**, *103*, 201115. [[CrossRef](#)]
59. Siriani, D.F.; Choquette, K.D. Implant defined anti-guided vertical-cavity surface-emitting laser arrays. *IEEE J. Quantum Electron.* **2011**, *47*, 160–164. [[CrossRef](#)]
60. Alias, M.S.; Shaari, S.; Leisher, P.O.; Choquette, K.D. Single transverse mode control of VCSEL by photonic crystal and trench patterning. *Photonics Nanostructures Fundam. Appl.* **2010**, *8*, 38–46. [[CrossRef](#)]
61. Siriani, D.F.; Choquette, K.D. Electronically controlled two-dimensional steering of in-phase coherently coupled vertical-cavity laser arrays. *IEEE Photonics Technol. Lett.* **2010**, *23*, 167–169. [[CrossRef](#)]
62. Gao, Z.; Thompson, B.J.; Dave, H.; Fryslie, S.T.; Choquette, K.D. Non-hermiticity and exceptional points in coherently coupled vertical cavity laser diode arrays. *Appl. Phys. Lett.* **2019**, *114*, 061103. [[CrossRef](#)]
63. Kominis, Y.; Choquette, K.D.; Bountis, A.; Kovanis, V. Exceptional points in two dissimilar coupled diode lasers. *Appl. Phys. Lett.* **2018**, *113*, 081103. [[CrossRef](#)]
64. Thompson, B.J.; Gao, Z.; Fryslie, S.T.; Choquette, K.D. Mode engineering in linear coherently coupled vertical-cavity surface-emitting laser arrays. *IEEE J. Sel. Top. Quantum Electron.* **2019**, *25*, 1701205. [[CrossRef](#)]
65. Dave, H.; Gao, Z.; Fryslie, S.T.M.; Thompson, B.J.; Choquette, K.D. Static and dynamic properties of coherently-coupled photonic-crystal vertical-cavity surface-emitting laser arrays. *IEEE J. Sel. Top. Quantum Electron.* **2019**, *25*, 1700208. [[CrossRef](#)]
66. Matsubara, H.; Yoshimoto, S.; Saito, H.; Jianglin, Y.; Tanaka, Y.; Noda, S. GaN photonic-crystal surface-emitting laser at blue-violet wavelengths. *Science* **2008**, *319*, 445–447. [[CrossRef](#)]
67. Lu, T.C.; Chen, S.W.; Kao, T.T.; Liu, T.W. Characteristics of GaN-based photonic crystal surface emitting lasers. *Appl. Phys. Lett.* **2008**, *93*, 111111. [[CrossRef](#)]
68. Bin, J.; Feng, K.; Shen, W.; Meng, M.; Liu, Q. Investigation on GaN-based membrane photonic crystal surface emitting lasers. *Materials* **2022**, *15*, 1479. [[CrossRef](#)] [[PubMed](#)]
69. Choi, Y.S.; Hennessy, K.; Sharma, R.; Haberer, E.; Gao, Y.; DenBaars, S.P.; Nakamura, S.; Meier, C. GaN blue photonic crystal membrane nanocavities. *Appl. Phys. Lett.* **2005**, *87*, 243101. [[CrossRef](#)]
70. David, A.; Fujii, T.; Moran, B.; Nakamura, S.; DenBaars, S.P.; Weisbuch, C.; Benisty, H. Photonic crystal laser lift-off GaN light-emitting diodes. *Appl. Phys. Lett.* **2006**, *88*, 133514. [[CrossRef](#)]
71. Hong, K.B.; Chen, L.R.; Huang, K.C.; Yen, H.T.; Weng, W.C.; Chuang, B.H.; Lu, T.C. Impact of air-hole on the optical performances of epitaxially regrown p-side up photonic crystal surface-emitting lasers. *IEEE J. Sel. Top. Quantum Electron.* **2021**, *28*, 9479706. [[CrossRef](#)]
72. Reuterskiöld Hedlund, C.; Martins De Pina, J.; Kalapala, A.; Liu, Z.; Zhou, W.; Hammar, M. Buried InP/air hole photonic-crystal surface-emitting lasers. *Phys. Status Solidi A* **2021**, *218*, 2000416. [[CrossRef](#)]
73. McKenzie, A.F.; King, B.C.; Rae, K.J.; Thoms, S.; Gerrard, N.D.; Orchard, J.R.; Nishi, K.; Takemasa, K.; Sugawara, M.; Taylor, R.J.E.; et al. Void engineering in epitaxially regrown GaAs-based photonic crystal surface emitting lasers by grating profile design. *Appl. Phys. Lett.* **2021**, *118*, 021109. [[CrossRef](#)]
74. Huang, Y.H.; Yang, Z.X.; Cheng, S.L.; Lin, C.H.; Lin, G.; Sun, K.W.; Lee, C.P. Effect of hole shift on threshold characteristics of gasb-based double-hole photonic-crystal surface-emitting lasers. *Micromachines* **2021**, *12*, 468. [[CrossRef](#)] [[PubMed](#)]
75. Bian, Z.; Rae, K.J.; King, B.C.; Kim, D.; Li, G.; Thoms, S.; Childs, D.T.D.; Gerrard, N.D.; Babazadeh, N.; Reynolds, P.; et al. Comparative analysis of void-containing and all-semiconductor 1.5  $\mu\text{m}$  InP-based photonic crystal surface-emitting laser diodes. *AIP Adv.* **2021**, *11*, 065315. [[CrossRef](#)]
76. Chen, L.R.; Hong, K.B.; Huang, K.C.; Liu, C.L.; Lin, W.; Lu, T.C. Study of an epitaxial regrowth process by MOCVD for photonic-crystal surface-emitting lasers. *Cryst. Growth Des.* **2021**, *21*, 3521–3527. [[CrossRef](#)]
77. Hirose, K.; Liang, Y.; Kurosaka, Y.; Watanabe, A.; Sugiyama, T.; Noda, S. Watt-class high-power, high-beam-quality photonic-crystal lasers. *Nat. Photonics* **2014**, *8*, 406–411. [[CrossRef](#)]

78. Williams, D.M.; Groom, K.M.; Stevens, B.J.; Childs, D.T.; Taylor, R.J.; Khamas, S.; Hogg, R.A.; Ikeda, N.; Sugimoto, Y. Epitaxially regrown GaAs-based photonic crystal surface-emitting laser. *IEEE Photonics Technol. Lett.* **2012**, *24*, 966–968. [[CrossRef](#)]
79. Hamamatsu Photonics, Photonic Crystal Surface Emitting Laser diodes (PCSEL). Available online: <https://www.hamamatsu.com/jp/en.html> (accessed on 23 April 2022).
80. Inoue, T.; Morita, R.; Yoshida, M.; De Zoysa, M.; Tanaka, Y.; Noda, S. Comprehensive analysis of photonic-crystal surface-emitting lasers via time-dependent three-dimensional coupled-wave theory. *Phys. Rev. B* **2019**, *99*, 035308. [[CrossRef](#)]
81. De Zoysa, M.; Yoshida, M.; Ishizaki, K.; Song, B.S.; Tanaka, Y.; Hatsuda, R.; Fukuhara, S.; Noda, S. 7W CW Operation of double-lattice photonic-crystal lasers. In Proceedings of the 2018 IEEE International Semiconductor Laser Conference (ISLC), Santa Fe, NM, USA, 16–19 September 2018; pp. 1–2.
82. Iadanza, S.; Liles, A.A.; Butler, S.M.; Hegarty, S.P.; O’Faolain, L. Photonic crystal lasers: From photonic crystal surface emitting lasers (PCSELS) to hybrid external cavity lasers (HECLs) and topological PhC lasers. *Opt. Mater. Express* **2021**, *11*, 3245–3274. [[CrossRef](#)]
83. Gao, X.; Yang, L.; Lin, H.; Zhang, L.; Li, J.; Bo, F.; Wang, Z.; Lu, L. Dirac-vortex topological cavities. *Nat. Nanotechnol.* **2020**, *15*, 1012–1018. [[CrossRef](#)] [[PubMed](#)]
84. Wang, Z.; Liang, Y.; Beck, M.; Scalari, G.; Faist, J. Topological charge of finite-size photonic crystal modes. *Phys. Rev. B* **2020**, *102*, 045122. [[CrossRef](#)]
85. Yoshida, M.; De Zoysa, M.; Ishizaki, K.; Kunishi, W.; Inoue, T.; Izumi, K.; Hatsuda, R.; Noda, S. Photonic-crystal lasers with high-quality narrow-divergence symmetric beams and their application to LiDAR. *J. Phys. Photonics* **2021**, *3*, 022006. [[CrossRef](#)]
86. Morita, R.; Inoue, T.; De Zoysa, M.; Ishizaki, K.; Noda, S. Photonic-crystal lasers with two-dimensionally arranged gain and loss sections for high-peak-power short-pulse operation. *Nat. Photonics* **2021**, *15*, 311–318. [[CrossRef](#)]
87. Takagi, S.; Tanimura, H.; Kakuno, T.; Hashimoto, R.; Kaneko, K.; Saito, S. Evaluation of thermal resistance of surface-emitting quantum cascade laser using structural function and 3D thermal flow simulation. In Proceedings of the 9th International Conference on Photonics, Optics and Laser Technology (PHOTOPTICS 2021), Online Streaming, 11–13 February 2021; pp. 88–93.
88. Guo, X.; Wang, Y.; Qi, A.; Qi, F.; Zhang, S.; Zheng, W. Photonic crystal surface emitting laser with ultralow thermal resistance and narrow divergence angle. In Proceedings of the 2016 Conference on Lasers and Electro-Optics (CLEO), San Jose, CA, USA, 5–10 June 2016.
89. Sciancalepore, C.; Bakir, B.B.; Seassal, C.; Letartre, X.; Harduin, J.; Olivier, N.; Fedeli, J.M.; Viktorovitch, P. Thermal, modal, and polarization features of double photonic crystal vertical-cavity surface-emitting lasers. *IEEE Photonics J.* **2012**, *4*, 399–410. [[CrossRef](#)]
90. Haghighat, G.; Ahmadi, V. Analysis of SHB and thermal characteristics in PC-VCSEL considering photonic crystal parameters. In Proceedings of the OSA Asia Communications and Photonics Conference, Shanghai, China, 13–16 November 2011; Volume 83082G.
91. Czyszanowski, T. Thermal properties and wavelength analysis of telecom oriented photonic-crystal VCSELs. *Opto-electron. Rev.* **2010**, *18*, 56–62. [[CrossRef](#)]
92. De Zoysa, M.; Yoshida, M.; Song, B.; Ishizaki, K.; Inoue, T.; Katsuno, S.; Izumi, K.; Tanaka, Y.; Hatsuda, R.; Gelleta, J.; et al. Thermal management for CW operation of large-area double-lattice photonic-crystal lasers. *JOSA B* **2020**, *37*, 3882–3887. [[CrossRef](#)]
93. Noda, S.; Yoshida, M.; Kunishi, W.; Inoue, T.; Ishizaki, K.; De Zoysa, M.; Kitamura, K.; Shimaji, N.; Nishimura, K. Photonic crystal lasers: Fabrication with AI-assisted technology and application to LiDAR system. *AI Opt. Data Sci. II SPIE* **2021**, *11703*, 117030M.
94. HELIOS+++Heidelberg LiDAR Operations Simulator. Available online: <https://www.geog.uni-heidelberg.de/gis/helios.html> (accessed on 28 April 2022).
95. Ito, K.; Niclass, C.; Aoyagi, I.; Matsubara, H.; Soga, M.; Kato, S.; Maeda, M.; Kagami, M. System design and performance characterization of a mems-based laser scanning time-of-flight sensor based on a 256 × 64-pixel single-photon imager. *IEEE Photonics J.* **2013**, *5*, 6800114. [[CrossRef](#)]
96. Alda, J. Laser and Gaussian beam propagation and transformation. *Encycl. Opt. Eng.* **2003**, 999–1013.